

# Force balance controls the relaxation time of the gradient descent algorithm in the satisfiable phase

Sungmin Hwang<sup>1</sup> and Harukuni Ikeda<sup>2,\*</sup>

<sup>1</sup>*LPTMS, Universit Paris-Sud 11, UMR 8626 CNRS, Bt. 100, 91405 Orsay Cedex, France*

<sup>2</sup>*Laboratoire de Physique de l'École Normale Supérieure, Université PSL, CNRS, Sorbonne Université, Université de Paris, 75005 Paris, France*

(Dated: November 22, 2019)

We numerically study the relaxation dynamics of the single layer perceptron with the spherical constraint. This is the simplest model of neural networks and serves a prototypical mean-field model of both convex and non-convex optimization problems. The relaxation time of the gradient descent algorithm rapidly increases near the SAT-UNSAT transition point. We numerically confirm that the first non-zero eigenvalue of the Hessian controls the relaxation time. This first eigenvalue vanishes much faster upon approaching the SAT-UNSAT transition point than the prediction of Marchenko-Pastur law in random matrix theory derived under the assumption that the set of unsatisfied constraints are uncorrelated. This leads to a non-trivial critical exponent of the relaxation time in the SAT phase. Using a simple scaling analysis, we show that the isolation of this first eigenvalue from the bulk of spectrum is attributed to the force balance at the SAT-UNSAT transition point. Finally, we show that the estimated critical exponent of the relaxation time in the non-convex region agrees very well with that of frictionless spherical particles, which have been studied in the context of the jamming transition of granular materials.

## I. INTRODUCTION

Constraint satisfaction problems (CSP) are ubiquitous in physics, chemistry, and engineering. Since the pioneering paper by Kirkpatrick *et. al.* [1], CSP have been studied extensively using tools of statistical mechanics [2, 3]. Although numerous studies have been done for CSP involving discrete degrees of freedom such as K-SAT [2, 3], the study of problems with continuous degrees of freedom is still in its infancy [4].

The standard approach of statistical mechanics is to first consider solvable mean-field models. Among several models of CSP with the continuous degrees of freedom, the perceptrons are probably most popular [5]. They are the simplest models of neural networks working as linear classifier of the given data set. If the size of input dataset is small, the system is in a satisfiable (SAT) phase where one can find neural weights that can perfectly classify the entire data. Contrary, if the size is too large, the system lies in the unsatisfiable (UNSAT) phase where no such solutions exist. In the thermodynamic limit, the SAT-UNSAT transition becomes a sharp phase transition at which several physical quantities exhibit singular behaviors [6].

The static equilibrium properties of the perceptron are now well-understood due to sophisticated mean-field theories such as the replica method [4, 6, 7]. However, their understanding of dynamics is still far from complete [8]. In this paper, we study the quenched dynamics of the perceptron through an extensive numerical simulation. We use the gradient descent dynamics (GDD), which is the most basic algorithm to optimize the cost function

of neural networks including the perceptrons [9, 10]. In particular, it is important to understand the dynamics in the SAT phase (*i.e.*, overparameterized phase) where the number of model parameters is larger than the number of input data. Many modern neural networks are trained in such regions [10], because overparameterized models can relax faster and avoid to get stuck in a bad local minima where the cost function has a higher value [11–16].

Another motivation to study the perceptron with the GDD is closely related to the dynamics of granular materials. The viscosity of driven granular particles diverges at a certain density, which is the so-called jamming transition [17]. It has been well-established that the jamming transition of spherical frictionless particles belongs to the same universality class of the SAT-UNSAT transition of the perceptron in the large dimensional limit [4, 7]. Interestingly, a recent numerical simulation of spherical particles driven by the GDD is proportional to the shear viscosity of the shear driven system near the jamming transition point [18]. This suggests that the perceptron driven by the GDD would be the simplest model to study the dynamics of the jamming transition.

In this work, by combining an extensive numerical simulation and scaling theory developed in Ref. [19], we show that the relaxation time in the SAT phase is controlled by the *unbalanced* force, which is the net force divided by the square root of the energy. By construction, the unbalanced force vanishes in the UNSAT phase, which leads to the divergence of the relaxation time when the system approaches to the SAT-UNSAT transition point from the SAT phase. Furthermore, interestingly, we find that the critical exponent obtained by our numerical simulation agrees very well with one of the theoretical prediction for the shear viscosity of spherical particles [19].

The paper is organized as follows. In Sec. II, we intro-

---

\* harukuni.ikeda@ens.fr

duce the model. In Sec. III, we show our numerical result for the relaxation dynamics. In Sec. IV, we discuss that an isolated eigenmode appears near the transition point, and this isolated mode controls the relaxation time. In Sec. V, we discuss the scaling theory of the isolated mode. Finally, in Sec. VI, we summarize and conclude the work.

## II. SETTING

### A. Model

In this work, we consider the generalized perceptron model investigated by Franz *et al.* [7]. In this section, we describe the detailed definition of the model in the context of the constraint satisfaction problem.

The perceptron model was originally introduced by Rosenblatt [5]. The aim of the perceptron is to correctly classify the input data. More precisely, one wants to find out the state variable  $\mathbf{X} = \{X_1, \dots, X_N\}$  such that

$$\text{sgn} \left[ \frac{1}{\sqrt{N}} \mathbf{X} \cdot \tilde{\boldsymbol{\xi}}^\mu \right] = y_\mu, \quad (1)$$

for all  $M$  input-output associations of  $\tilde{\boldsymbol{\xi}}^\mu = \{\tilde{\xi}_1^\mu, \dots, \tilde{\xi}_N^\mu\}$  and  $y_\mu \in \{-1, 1\}$  where  $\mu$  is an index running from 1 to  $M$ . Since these constraints are scale-independent, it is natural to introduce a regularization condition

$$\mathbf{X} \cdot \mathbf{X} = N. \quad (2)$$

to prevent an overflow through the dynamics. Additionally, let us consider the case where  $\tilde{\xi}_i^\mu$  is a Gaussian random variable with zero mean and unit variance.

The classification problem above can be recast into a constraint satisfaction problem with the following constraints

$$h_\mu = \frac{y_\mu}{\sqrt{N}} \mathbf{X} \cdot \tilde{\boldsymbol{\xi}}^\mu = \frac{1}{\sqrt{N}} \mathbf{X} \cdot \boldsymbol{\xi}^\mu \geq 0, \quad (3)$$

where we have introduced new random variables  $\boldsymbol{\xi}^\mu = y_\mu \tilde{\boldsymbol{\xi}}^\mu$ , which has the same distribution of the original one. A conventional approach to solve this problem is to translate it into an optimization problem with a corresponding cost function

$$H = \sum_{\mu=1}^M \frac{h_\mu^2}{2} \theta(-h_\mu), \quad (4)$$

where  $\theta(x)$  denotes the Heaviside step function. This cost function is designed in such a way that it vanishes  $H = 0$  if and only if  $\mathbf{X}$  satisfies all the constraints Eq. (3).

The typical case performance of the perceptron can be studied by calculating the typical value of  $H$  at zero temperature, which is tantamount to studying the ground state energy of the model where the interaction among state variables  $X_i$ 's are given by the Hamiltonian  $H$ . This detailed thermodynamic study uncovers a sharp phase

transition in the thermodynamics limit from a satisfiable (SAT) phase, where one can find  $\mathbf{X}$  such that  $H = 0$ , to an unsatisfiable (UNSAT) phase, where there are no such configurations and thus  $H > 0$  [2].

The cost function of the original perceptron model can be shown to be convex, and thus to form a single cluster of solutions. However, in many realistic problems, such as the state of the art multilayer neural networks used in machine learning algorithms, the corresponding optimization problems are not necessarily convex and the cost function can have many metastable states [10]. To investigate the effect of non-convexity, Franz *et al.* [7] introduced a variant of the standard perceptron with the following modified constraints:

$$h_\mu = \frac{1}{\sqrt{N}} \mathbf{X} \cdot \boldsymbol{\xi}^\mu - \sigma \geq 0, \quad \mu = 1, \dots, M, \quad (5)$$

where  $\sigma$  is referred to as the bias. The original problem corresponds to  $\sigma = 0$ . One can define the cost function as Eq. (4), and calculate the phase diagram as a function of  $\sigma$  and  $\alpha = M/N$  by using the replica method. As in the case of the standard perceptron, the model exhibits the SAT-UNSAT transition at  $\alpha = \alpha_c$  at which  $H$  begins to have a non-zero value [7]. When  $\sigma \geq 0$ , the cost function has a single minimum, and thus the optimization problem is convex as in the case of the standard perceptron [6]. On the contrary, when  $\sigma < 0$ , the cost function begins to have an exponential number of metastable states near  $\alpha_c$ , meaning that the problem is non-convex [4, 7].

The static critical behavior of the perceptron in the non-convex region  $\sigma < 0$  has been fully investigated using the replica method. At the SAT-UNSAT transition point, the theory predicts that (i) the system becomes isostatic at the SAT-UNSAT transition point, meaning that the contact number is the same of that of the number of degrees of freedom [4], (ii) the two point correlation function exhibits power law scaling, for instance, the two point force distribution has a pseudo gap  $P(f) \sim f^\theta$  with  $\theta = 0.423$  for small force  $f$  [4], and (iii) the eigenvalue distribution is gapless in the UNSAT phase [20].

### B. Dynamics

We consider the simple GDD:

$$\frac{d\mathbf{X}(t)}{dt} = -P(t) \cdot \nabla H, \quad (6)$$

where  $\nabla_i = \partial/\partial X_i$ , and

$$P_{ij}(t) = \delta_{ij} - \frac{1}{N} X_i(t) X_j(t) \quad (7)$$

denotes the projection operator onto a hypersphere defined by Eq. (2). Using Eq. (6), one can show that

$$\dot{\mathbf{X}}(t) \cdot \dot{\mathbf{X}}(t) = 0, \quad (8)$$

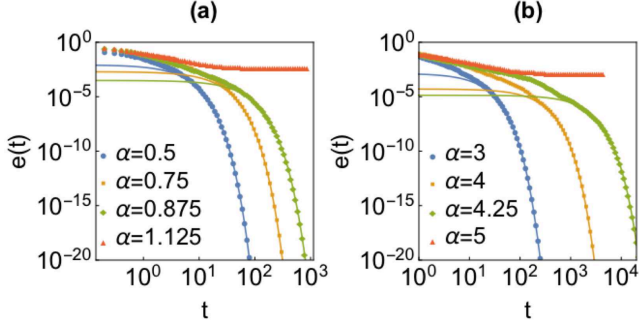


FIG. 1. Time evolution of the energy as a function of time (a) in a convex regime  $\sigma = 0.5$  and (b) in a non-convex regime  $\sigma = -0.5$ . The markers denote the numerical results of single trajectory for each parameter. The solid lines denote the exponential fit.

suggesting that the constraint Eq. (2) is automatically satisfied if  $\mathbf{X}(0) \cdot \mathbf{X}(0) = N$ . For the numerical integration, we have to discretize Eq. (6) without violating Eq. (2). For this purpose, we consider the following discretized dynamics:

$$\begin{aligned} \mathbf{Y}(t + \Delta t) &= \mathbf{X}(t) - \Delta t \nabla H, \\ \mathbf{X}(t + \Delta t) &= \sqrt{N} \frac{\mathbf{Y}(t + \Delta t)}{\sqrt{\mathbf{Y}(t + \Delta t) \cdot \mathbf{Y}(t + \Delta t)}}, \end{aligned} \quad (9)$$

where  $\Delta t$  denotes the time step. One can show that Eq. (9) agrees with Eq. (6) up to the first order of  $\Delta t$ .

### C. Details of numerics

For the initial condition  $\mathbf{X}(0)$ , we generate a uniform random configuration on the  $N$  dimensional hypersphere so that  $\mathbf{X}(0) \cdot \mathbf{X}(0) = N$ . Starting from this configuration, we evolve the system by applying Eq. (9) iteratively. We define the time as  $t = \Delta t N_{\text{step}}$  where  $N_{\text{step}}$  denotes the number of the iteration. We stop the iteration when

$$f_p \equiv \sqrt{\frac{1}{N} \sum_{i=1}^N (P \nabla H)_i^2} < 10^{-10}. \quad (10)$$

We use  $\Delta t = 0.1$  and  $N = 256$  unless otherwise noted. Hereafter we mostly show numerical results for  $\sigma = 0.5$ , where the cost function is convex, and  $\sigma = -0.5$ , where the cost function is non-convex.

## III. RELAXATION

### A. Time evolution of physical quantities

First, we report the time evolution of several physical quantities. In Fig. 1 (a), we show the time dependence of the cost function per particle  $e(t) = H(t)/N$  for  $\sigma = 0.5$

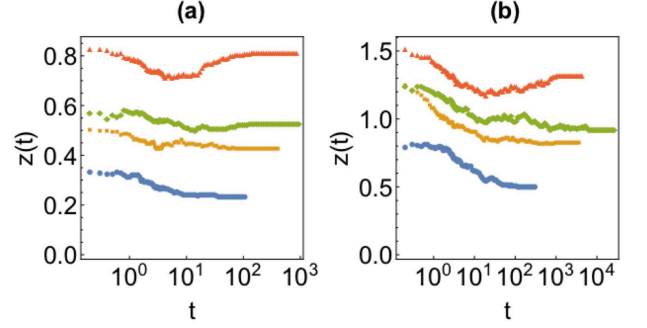


FIG. 2. Time dependence of the contact number. The markers denote the numerical results of single trajectory for each parameter. The values of  $\alpha$  are the same as Fig. 1. (a) The results for the convex problem  $\sigma = 0.5$ . (b) The result for the non-convex problem  $\sigma = -0.5$ .

where the static replica calculation predicts that the cost function is convex [4]. For small  $\alpha$ ,  $e(t)$  decreases monotonically to zero, see the data for  $\alpha = 0.5, 0.75$ , and  $0.875$  in Fig. 1 (a). This indicates that the system lies in a SAT phase. The late time behavior of  $e(t)$  can be well fitted by an exponential function (see the solid lines in Fig. 1 (a)). On the contrary, for the larger values of  $\alpha$ ,  $e(t)$  does not decay to zero in the long time limit, indicating that the system lies in an UNSAT phase (see the data for  $\alpha = 1.125$  in Fig. 1 (a)). In Fig. 1 (b), we show  $e(t)$  for  $\sigma = -0.5$  where the cost function is non-convex [4]. Despite this difference, the relaxation of  $e(t)$  is quite similar to that of the convex case ( $\sigma = 0.5$ ). Namely,  $e(t)$  exhibits an exponential decay for small  $\alpha$ , (see the data for  $\alpha = 3, 4$ , and  $4.25$ ), while it converges to a finite value for larger  $\alpha$ 's, (see the data for  $\alpha = 5$ ). Further studies, such as the investigation of the aging dynamics, are necessary to clarify the qualitative difference of the relaxation dynamics between the convex and non-convex problems. We leave it for future work.

The other important quantity is the contact number  $z(t)$ , namely, the number of unsatisfied constraints:

$$z(t) = \frac{1}{N} \sum_{\mu=1}^M \theta(-h_{\mu}). \quad (11)$$

In Fig. 2 (a), we show the time evolution of  $z(t)$  for  $\sigma = 0.5$  and the same values of  $\alpha$  as Fig. 1 (a).  $z(t)$  converges to a finite value in the long time limit:

$$z \equiv \lim_{t \rightarrow \infty} z(t). \quad (12)$$

$z$  tends to smoothly increase with  $\alpha$ . It may be a little counter intuitive that  $z$  has a finite value even in the SAT phase where  $e \equiv \lim_{t \rightarrow \infty} e(t) = 0$ . However, this is a natural consequence of the GDD Eq. (6) and definition of  $z(t)$  Eq. (11). Since the dynamics does not involve inertia, some contacts converge to  $h_{\mu} \rightarrow 0^-$ , implying that  $\theta(-h_{\mu}) = 1$  even in the long time limit [18].

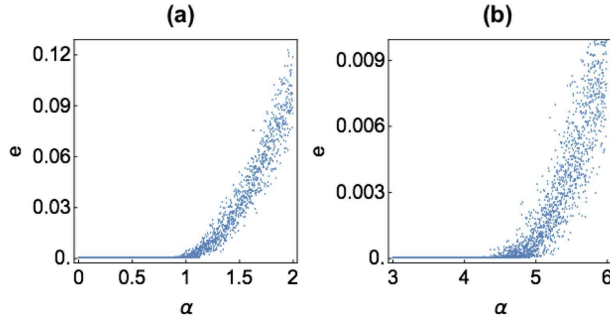


FIG. 3.  $\alpha$  dependence of the energy per particle at the stationary state. The markers denote the numerical results measured for each individual configuration. (a) Numerical results in the convex phase. (b) Numerical results in the non-convex phase.

### B. Physical quantities at the stationary state

Next, we shall study  $e(t)$  and  $z(t)$  in the long time limit,  $e \equiv \lim_{t \rightarrow \infty} e(t)$  and  $z \equiv \lim_{t \rightarrow \infty} z(t)$ . To obtain the stationary state configuration, we run numerical simulations for various values of  $\alpha$  and initial conditions until Eq. (10) is satisfied. Then, we calculate the energy  $e(t)$  and the contact number  $z(t)$  at the stationary state.

In Fig. 3 (a), we show the stationary state energy  $e$  for the convex case  $\sigma = 0.5$ . For small  $\alpha$ , the zero energy  $e = 0$  suggests that the system lies in a SAT phase. The energy  $e$  begins to have a non-zero value at  $\alpha = \alpha_c \approx 1$ , which is the signature of the SAT-UNSAT transition. The transition point well agrees with the theoretical prediction  $\alpha_c = 0.961$  [4]. In Fig. 3 (b), we show the numerical result for the non-convex case  $\sigma = -0.5$ . The SAT-UNSAT transition takes place at  $\alpha_c \approx 4.5$ . This is close to the theoretical prediction within the RS Ansatz  $\alpha_c = 4.77$  [4]. Strictly speaking, in a convex phase, the RS Ansatz becomes unstable, and thus one should take into account a more complex RSB Ansatz. Interestingly, the above result suggests that the RS Ansatz already gives a good approximation value for the transition point [21]

In Fig. 4 (a), we show the contact number of the stationary state  $z$  for the case of the convex problem ( $\sigma = 0.5$ ).  $z$  tends to increase in  $\alpha$  and develops a non-analytic point exactly at the SAT-UNSAT transition. The numerical results of  $z$  at  $\alpha_c$  well agrees with the theoretical prediction  $z(\alpha_c) = 0.665$ , i.e., the horizontal lines originally computed in [4]. In Fig. 4 (b), we show  $z$  for the case of the non-convex problem ( $\sigma = -0.5$ ). The theory predicts that for  $\sigma < 0$ , the system becomes isostatic at the transition point,  $z(\alpha_c) = 1$  [4]. The numerical result agrees well with this prediction, see the horizontal line in Fig. 4 (b).

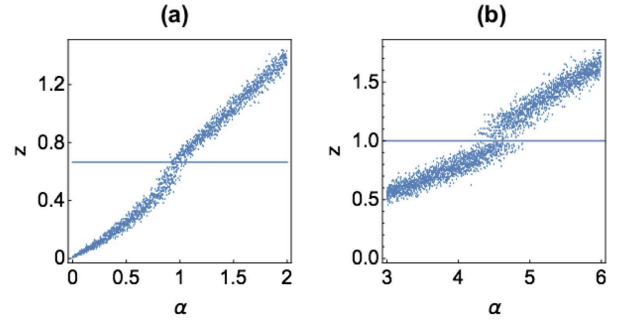


FIG. 4.  $\alpha$  dependence of the contact number per particle at the stationary state. The markers denote the numerical results measured for each individual configuration. The solid line denotes the theoretical prediction of  $z$  at the SAT-UNSAT transition point. (a) Numerical results in the convex phase. (b) Numerical results in the non-convex phase.

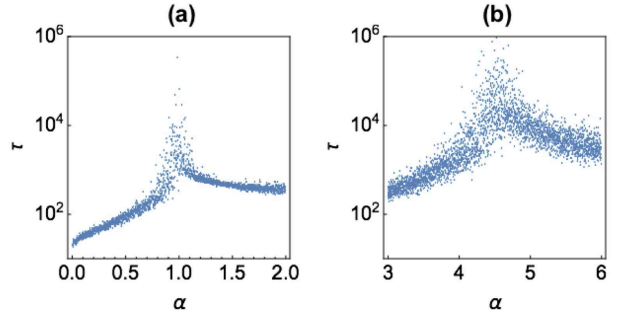


FIG. 5.  $\alpha$  dependence of the relaxation time. The markers denote the numerical results measured for each individual configuration. (a) The result in the convex phase. (b) The result in the non-convex phase.

### C. Relaxation time

Finally, we discuss the  $\alpha$  dependence of the relaxation time. We define the relaxation time  $\tau$  as the time when the system first satisfies the stationary state condition Eq. (10).

In Fig. 5, we show the  $\alpha$  dependence of  $\tau$  for both a convex regime ( $\sigma = 0.5$ ) and a non-convex regime ( $\sigma = -0.5$ ). The relaxation time  $\tau$  exhibits a sharp peak at the SAT-UNSAT transition point (a)  $\alpha_c \approx 1$  and (b)  $\alpha_c \approx 4.5$ . These results prove that the SAT-UNSAT transition is a critical phenomenon accompanied by the divergence of the relaxation time. Below, we show that this divergence is a consequence of vanishing first nonzero eigenvalue of the Hessian of the cost function.

## IV. EIGENMODES OF HESSIAN

We here investigate the eigenvalues of the Hessian constructed from a second-order approximation of the cost function evaluated at the stationary point. In a SAT



phase, the stationary point is formed at a boundary of solution space due to a lack of inertia. Thus, one can naturally expect that there exist many zero modes along the directions towards islands of solutions while there are also non-zero modes coming from the contributions of infinitesimally unsatisfied patterns at the boundary. If these patterns are statistically uncorrelated, one can immediately show that the spectrum of such Hessian follows a Marchenko-Pastur law [20].

Strikingly, one of our main findings is to show that the first non-zero eigenmode is an outlier when compared against this null model. Specifically, we found that the eigenvalue is statistically much smaller than the bulk spectrum which cannot be explained by a usual Tracy-Widom distribution. This implies that our dynamics chooses the set of unsatisfied patterns in such a way that they form a non-trivial correlation. Because the dynamics should be well approximated by a corresponding Hessian dynamics at least near the boundary, we can conclude that the dynamics is significantly slower than that of relaxation dynamics of random patterns.

#### A. Derivation of the Hessian at the stationary state in the SAT phase

We expand the cost function around the stationary state  $\mathbf{X}_*$  as follows

$$\begin{aligned}\delta H &= H(\mathbf{X}_* + P\boldsymbol{\varepsilon}) - H(\mathbf{X}_*) \\ &\approx P\boldsymbol{\varepsilon} \cdot \nabla H + \frac{1}{2} [P\boldsymbol{\varepsilon} \cdot \nabla (P\boldsymbol{\varepsilon} \cdot \nabla H)] \\ &= \boldsymbol{\varepsilon} \cdot P \cdot \nabla H + \frac{1}{2} \boldsymbol{\varepsilon} \cdot M \cdot \boldsymbol{\varepsilon}\end{aligned}\quad (13)$$

where  $P$  denotes the projection operator defined by Eq. (7). One can always eliminate the anti-symmetric part of  $M$  in Eq. (13) and express it as a symmetric matrix

$$\begin{aligned}M_{ij} &= \frac{1}{2} \sum_{n,m=1}^N \left[ P_{in} \frac{\partial}{\partial X_n} \left( P_{jm} \frac{\partial H}{\partial X_m} \right) \right. \\ &\quad \left. + P_{jn} \frac{\partial}{\partial X_n} \left( P_{im} \frac{\partial H}{\partial X_m} \right) \right] \\ &= (P \cdot \nabla^2 H \cdot P)_{ij} + \zeta P_{ij} - \frac{(P \nabla H)_i X_j + X_i (P \nabla H)_j}{2N},\end{aligned}\quad (14)$$

where we have introduced an auxiliary variable

$$\zeta = -\frac{1}{N} \mathbf{X} \cdot \nabla H = -\frac{1}{N} \sum_{\mu=1}^M \theta(-h_\mu) (h_\mu^2 + \sigma h_\mu). \quad (16)$$

At the stationary state, we have  $(P \nabla H(\mathbf{X}_*))_i = \sum_{n=1}^N P_{in} \nabla_n H = 0$ . Also, in the SAT phase,  $h_\mu \rightarrow 0$

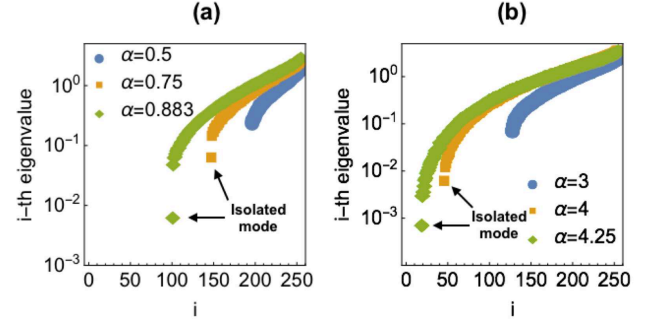


FIG. 6. The typical spectrum of Hessian matrices shown in rank plots. The markers denote the numerical results of one configuration for each parameter. Zero modes are excluded from the plots. (a) The results for the convex problem ( $\sigma = 0.5$ ). (b) The result for the non-convex problem ( $\sigma = -0.5$ ).

which leads to  $\zeta = 0$ . Under such conditions, the Hessian matrix  $\mathcal{H}$  can be simply expressed as

$$\mathcal{H}_{ij} = \frac{1}{N} (P \cdot \nabla^2 H \cdot P)_{ij} = \frac{1}{N} \sum_{\mu=1}^M \theta(-h_\mu) (P \boldsymbol{\xi}^\mu)_i (P \boldsymbol{\xi}^\mu)_j. \quad (17)$$

Note that this expression is different from the one studied in the equilibrium dynamics in Ref. [22] where authors considered the Hessian of the free energy.

#### B. Zero modes

There are  $N(1 - z)$  number of linearly independent vectors  $\mathbf{e}_l$ ,  $l = 1, \dots, N(1 - z)$  that satisfy  $\mathbf{e}_l \cdot P \boldsymbol{\xi}^\alpha = 0$  for  $\alpha = 1, \dots, Nz$ , where  $z$  denotes the number of contacts normalized by  $N$  at the stationary state given by Eqs. (11) and (12), and  $\boldsymbol{\xi}^\alpha$  denotes the contact that satisfies  $h_\alpha \leq 0$ . From Eq. (17), it follows that

$$\mathcal{H} \mathbf{e}_l = 0, \quad (18)$$

meaning that  $\mathbf{e}_l$  is a zero eigenvector of  $\mathcal{H}$ . Since the system does not evolve along the direction of the zero modes, hereafter we neglect the zero modes.

#### C. Isolated eigenmode

In Fig. 6 (a) and (b), we show the typical behavior of the eigenvalues at the stationary state in the SAT phase for the case of the convex problem ( $\sigma = 0.5$ ) and non-convex problem ( $\sigma = -0.5$ ), respectively. In the SAT phase, there are  $N(1 - z)$  number of zero modes (not shown). As  $\alpha$  approaches  $\alpha_c$ , the first nonzero eigenvalue  $\lambda_1$  decreases much faster than the other eigenvalues, suggesting that  $\lambda_1$  is the isolated eigenvalue near  $\alpha_c$  for both convex and non-convex problems.

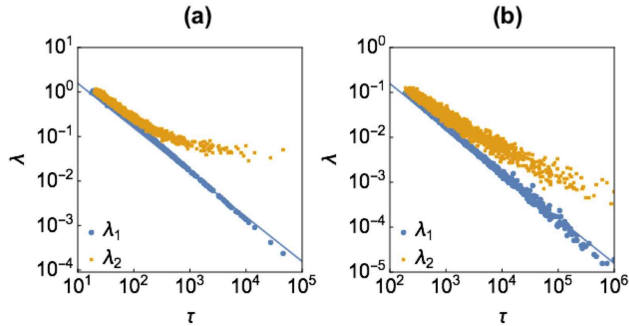


FIG. 7. Scatter plots of the first/second non-zero eigenvalues and the relaxation time. The markers denote the numerical results measured for each individual configuration. The solid line indicates  $\lambda \propto \tau^{-1}$ . (a) The results for the convex problem ( $\sigma = 0.5$ ). (b) The result for the non-convex problem ( $\sigma = -0.5$ ).

#### D. Eigenvalues and relaxation time in the SAT phase

In Fig. 7 (a) and (b), we show the scatter plots of the first and second eigenvalues,  $\lambda_1$  and  $\lambda_2$ , against the relaxation time  $\tau$  in the SAT phase. One can clearly see that  $\tau$  is inversely proportional to  $\lambda_1$ :

$$\tau \sim \lambda_1^{-1}. \quad (19)$$

This is a direct evidence of the fact that  $\lambda_1$  controls the GDD near the SAT-UNSAT transition point. The second smallest eigenvalue  $\lambda_2$  behaves similarly to  $\lambda_1$  for small  $\tau$ , while it starts to deviate from  $\lambda_1$  as  $\tau$  increases. This implies that the separation of  $\lambda_1$  and  $\lambda_2$  becomes more pronounced as the system approaches the transition point. This is consistent with the results shown in Fig. 6, where the first eigenvalue is isolated near the transition point.

#### E. Scaling of the first eigenvalue

Recent numerical studies of a particle system reveal that the relaxation time  $\tau$  of the quenched system is proportional to the shear viscosity  $\eta$  near the jamming transition point, if one plots both quantities as a function of the contact number [18]. This motivates us to study the scaling of  $\tau$  of the perceptron for  $\sigma < 0$  where the model belongs to the same universality class of spherical particles in the large dimensional limit [7]. As discussed in the previous section,  $\tau$  is inversely proportional to  $\lambda_1$ . Therefore, instead of  $\tau$ , we here calculate  $\lambda_1$  as a function of the contact number  $z$ . We perform extensive numerical simulations for various initial configurations and for different values of  $\alpha$ . Obviously, each different setting will find a different value of  $z$  in the stationary limit. Thus, we calculate the mean value of  $\lambda_1$  averaged over

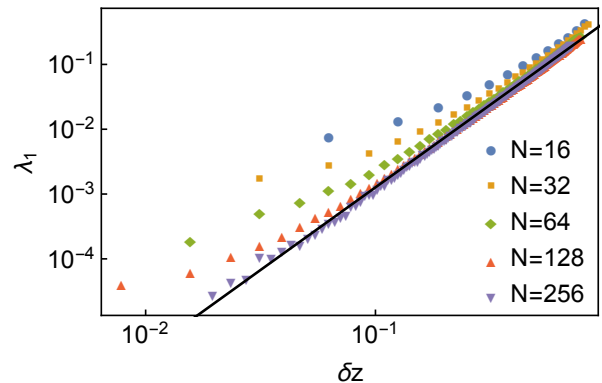


FIG. 8. Scaling of  $\lambda_1$  for  $\sigma = -0.5$ . The markers denote the numerical results of the average value of  $\lambda_1$ , while the solid line denotes the prediction of the finite size scaling  $\lambda_1 \sim \delta z^{2.55}$ .

the samples with the same value of  $z$ . We collected at least 10 samples for each  $z$ .

In Fig. 8, we show our numerical results of  $\lambda_1$  as a function of the deficit contact number

$$\delta z = 1 - z. \quad (20)$$

For the non-convex region ( $\sigma < 0$ ), the perceptron becomes isostatic  $\delta z = 0$  at the transition point [4]. We find that  $\lambda_1$  exhibits power law scaling for the intermediate value of  $\delta z$ . For very small  $\delta z$ , however,  $\lambda_1$  deviates from the power law and converges to a finite value. The power law region persists longer as  $\delta z \rightarrow 0$  for larger  $N$ , suggesting that the deviation from the power law is a finite size effect.

In order to determine the critical exponent precisely, we perform a finite size scaling analysis. Following the scaling argument above the jamming transition point [23], we assume that  $\lambda_1 \sim \delta z^\beta$  for  $\delta z \gg 1/N$ , while  $\lambda_1$  converges to a finite value for  $\delta z \sim 1/N$ . This assumption leads to the following scaling function for finite  $N$  systems:

$$\lambda_1(N, \delta z) \sim N^{-\beta} f_1(N\delta z), \quad (21)$$

where  $f_1(x) \sim x^\beta$  for  $x \gg 1$ , and  $f_1(x) \sim x^0$  for  $x \sim 1$ . In Fig. 9 (a), we show the  $N$  dependence of  $\lambda_1$  for  $\delta z = 1/N$ . As expected from Eq. (21), the data are well fitted by a power law  $\lambda_1 \sim N^{-\beta}$  with a critical exponent

$$\beta = 2.55 \pm 0.15. \quad (22)$$

In Fig. 9 (b), we show a scaling plot predicted by Eqs. (21) and (22). The excellent collapse of the data for different  $N$  strongly supports our scaling analysis.

### V. SCALING THEORY

In this section, we try to identify the origin of the isolated mode and derive the analytic expression of the dynamical critical exponent  $\beta$ .

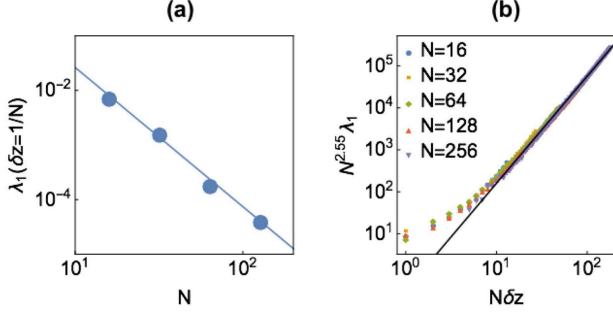


FIG. 9. Finite  $N$  scaling of  $\lambda_1$  for  $\sigma = -0.5$ . (a)  $N$  dependence of  $\lambda_1$  for  $\delta z = 1/N$ . The markers denote the numerical result, while the solid line denotes the result of the power law fit  $\lambda_1 \sim N^{-2.55}$ . (b) Scaling plot of the same data as Fig. 8.

### A. Unbalanced force controls the isolated mode

Here we discuss that the force balance at the SAT-UNSAT transition point leads to the vanishing behavior of  $\lambda_1$ . For this purpose, we consider the linearized equation around the stationary state  $\delta \dot{\mathbf{X}}(t) \approx -\mathcal{H} \delta \mathbf{X}(t)$ , where  $\delta \mathbf{X}(t) = \mathbf{X}(t) - \mathbf{X}_*$ , and  $\mathbf{X}_*$  denotes the configuration at the stationary state. In the long time limit,  $\delta \mathbf{X}(t)$  converges to the eigenvector of the first non-zero eigenvalue  $\lambda_1$ , therefore we have  $\delta \dot{\mathbf{X}}(t) \sim -\lambda_1 \delta \mathbf{X}(t)$ , which leads to

$$|\delta \mathbf{X}(t)| \sim e^{-\lambda_1 t}. \quad (23)$$

Similarly, the cost function is  $H(t) \sim |\delta \mathbf{X}(t)|^2 \sim e^{-2\lambda_1 t}$ , which allows us to express  $\lambda_1$  as

$$\begin{aligned} \lambda_1 &= -\frac{1}{2} \lim_{t \rightarrow \infty} \frac{\dot{H}(t)}{H(t)} = \left. \frac{\sum_i (P \nabla H)_i^2}{2H} \right|_{\mathbf{X}=\mathbf{X}_*} \\ &\equiv \frac{1}{N} \sum_{i=1}^N F_i^2. \end{aligned} \quad (24)$$

Here we have introduced the *unbalanced force* as

$$F_i = \sum_{\mu=1}^M \theta(f_\mu) \frac{1}{\sqrt{N}} (P \xi^\mu)_i f_\mu, \quad f_\mu = -\frac{h_\mu}{\sqrt{\langle h^2 \rangle}}. \quad (25)$$

$\mathbf{F} = \{F_1, \dots, F_N\}$  is the eigenvector of  $\lambda_1$ , because  $\mathbf{F} \propto P \nabla H \propto \mathcal{H} \delta \mathbf{X}$ , and  $\delta \mathbf{X}$  converges to the eigenvector of  $\lambda_1$ . In Fig. 10, we numerically confirm the validity of Eq. (24).

In the UNSAT phase,  $F_i = 0$  because  $H > 0$  and  $P \nabla H = 0$  at the stationary state. On the contrary, in the SAT phase,  $F_i$  can have a finite value because both  $H$  and  $P \nabla H$  vanish at the stationary state. From the continuity of  $F_i$ , it follows that  $F_i = 0$  at the SAT-UNSAT transition point, which leads to  $\lambda_1 = 0$  and the divergence of the relaxation time  $\tau$ . It is worth noting that the above scenario, where the force balance controls the slow dynamics near the transition point, holds not only for the perceptron but also for more general models driven by the GDD both in the convex and non-convex phases.

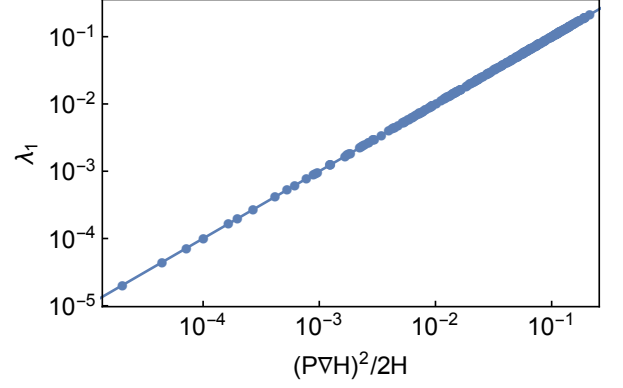


FIG. 10. Scatter plot of  $\lambda_1$  and  $(P \nabla H)^2 / (2H)$  for  $\sigma = -0.5$ . The markers denote the numerical results measured for each individual configuration. The solid line denotes the theoretical prediction  $\lambda_1 = (P \nabla H)^2 / 2H$ .

### B. Variational argument

Now we derive the scaling of  $\lambda_1$  using the assumption of the marginal stability [24]. When the quench rate is increased, the system arrives at less stable state. In particular, for the GDD, which corresponds to the infinitely fast quench, the system would reach the most unstable configuration for the given constraints. More concretely, for our model, among possible configurations with fixed  $z$ , the one with the smallest  $\lambda_1$  would be realized:

$$\lambda_1 = \min_{\text{fixed } z} \frac{1}{N} \sum_{i=1}^N F_i^2. \quad (26)$$

Following Ref. [19], we shall construct the configuration satisfying Eq. (26) by removing the contacts from the isostatic configuration where  $\delta z = 0$  and  $\lambda_1 = 0$ . Removing the contacts would break the force balance, leading to  $F_i > 0$  and  $\lambda_1 > 0$ . In order to minimize  $\lambda_1$ , one should minimize the perturbation from the isostatic configuration. This would be possible by removing the weakest contacts that have the smallest values of  $f_\mu$ . The typical force scale of the weakest contacts is

$$f_{\text{av}} \equiv \frac{\int_0^{f_*} P(f) f df}{\int_0^{f_*} P(f) df} \sim f_*, \quad (27)$$

where  $P(f) \sim f^\theta$  with  $\theta = 0.423$  denotes the force distribution at jamming [4, 25], and the upper bound  $f_*$  is calculated by using the extreme statistics as follows

$$\int_0^{f_*} P(f) df \sim \delta z \rightarrow f_* \sim \delta z^{\frac{1}{1+\theta}}. \quad (28)$$

When the  $N\delta z$  number of the weakest contacts are removed, we have

$$|F_i| \sim \left| -\frac{1}{\sqrt{N}} \sum_{\alpha=1}^{N\delta z} (P\xi^{\mu_\alpha})_i f_{\mu_\alpha} \right| \sim \frac{f_{\text{av}}}{\sqrt{N}} (N\delta z)^{1/2} \sim f_* \delta z^{1/2}, \quad (29)$$

where  $\mu_\alpha$  denotes the suffix of the weakest contacts. Here we have assumed that  $f_{\mu_\alpha}$  is uncorrelated with  $(P\xi^{\mu_\alpha})_i$  and replaced it by its average value. Substituting Eq. (29) into Eq. (26), we finally arrive to

$$\lambda_1 \sim f_*^2 \delta z \sim \delta z^{\frac{3+\theta}{1+\theta}}. \quad (30)$$

Interestingly, despite the difference of the dynamics and model, the same result was previously derived for spherical particles driven by shear [19]. Using the result of the static replica calculation  $\theta = 0.423$  [4, 25], we have a theoretical prediction for the dynamical critical exponent

$$\beta_{\text{theory}} = \frac{3+\theta}{1+\theta} = 2.41. \quad (31)$$

This is reasonably close to the numerical result Eq. (22).

In Eq. (29), we used the central limit theorem to replace the summation of the  $N\delta z$  random variables by  $(N\delta z)^{1/2}$ . This would be verified if  $N\delta z \gg 1$ . On the contrary, if  $N\delta z \approx 1$ , Eq. (29) and the scaling Eq. (30) do not hold. In other words, the finite  $N$  effects appear at  $\delta z \sim 1/N$ , which supports the scaling form Eq. (21) used for the finite size scaling analysis.

### C. Scaling of the second eigenvalue

In the previous subsection, we have discussed that the unbalanced force controls the first eigenmode in the satisfiable phase. At the transition point, the unbalanced force vanishes, which yields a strong correlation between  $\xi^\mu$  along the direction of the unbalanced force  $\mathbf{F}$ . For the directions orthogonal to  $\mathbf{F}$ , there are no such constraints. Thus, we can assume that  $(P\xi^\mu)_i$  are uncorrelated with each other. In this case, the Hessian, Eq. (17), can be identified by a Wishart matrix [26]. The eigenvalue distribution  $\rho(\lambda)$  is given by the Marchenko-Pastur distribution [20]:

$$\rho(\lambda) = (1-z)\delta(\lambda) + \frac{1}{2\pi} \frac{\sqrt{(\lambda - \lambda_-)(\lambda_+ - \lambda)}}{\lambda}, \quad (32)$$

where

$$\lambda_{\pm} = (\sqrt{z} \pm 1)^2. \quad (33)$$

We believe that it would correctly describe the continuous part of the spectrum. In Fig. 6, we saw that the second eigenvalue  $\lambda_2$  is the lowest eigenvalue of the continuous spectrum. Therefore, from Eqs. (32) and (33), we expect for  $\delta z \ll 1$

$$\lambda_2 \sim \lambda_- \sim \delta z^2. \quad (34)$$

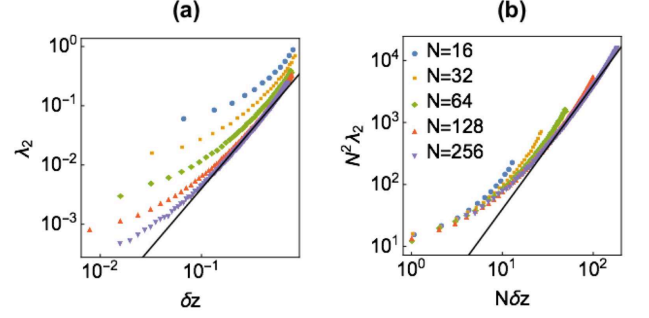


FIG. 11. Scaling of the second eigenvalue  $\lambda_2$  for  $\sigma = -0.5$ . (a) The markers denote the numerical results of the average value of  $\lambda_2$ . The solid lines denote the power law  $\lambda_2 \sim \delta z^2$ . (b) The scaling plot of the same data.

This expression is valid in the thermodynamic limit. For finite  $N$ , we put a similar Ansatz as Eq. (21):

$$\lambda_2(N, \delta z) \sim N^{-2} f_2(N\delta z), \quad (35)$$

where  $f_2(x) \sim x^2$  for  $x \gg 1$ , and  $f_2(x) \sim x^0$  for  $x \sim 1$ . In Fig. 11 (a), we show the numerical result of  $\lambda_2$  as a function of  $\delta z$ . One can see that  $\lambda_2$  exhibits power law scaling  $\lambda_2 \sim \delta z^2$  for intermediate values of  $\delta z$ . The power law region increases with  $N$ . In Fig. 11 (b), we show the scaling plot of the same data. The excellent collapse of the data of different  $N$  confirms Eq. (35).

The above analysis shows that the first eigenmode  $\lambda_1$  and the continuous part of the spectrum are controlled by the completely different mechanisms, which may explain the isolation of  $\lambda_1$ .

## VI. SUMMARY AND DISCUSSIONS

In this work, we numerically studied the critical dynamics of the perceptron near the SAT-UNSAT transition point. The relaxation time is inversely proportional to the first non-zero eigenvalue  $\lambda_1$ . As the system approaches the transition point,  $\lambda_1$  vanishes much faster than the continuous part of the spectrum. We discussed that  $\lambda_1$  is controlled by the unbalanced force which vanishes at the transition point by construction. We then calculated the critical exponent of  $\lambda_1$  in the non-convex phase where the model has the same universality as that of the spherical particles in the large dimensional limit. We found  $\lambda_1 \sim \delta z^{2.55}$ , which is very close to the previous analytical result of frictionless spherical particles driven by the external shear near the jamming transition point [19].

One of our main findings is that the isolated mode robustly appears in the SAT phase in the proximity of the SAT-UNSAT transition point both in the case of convex and non-convex problems. This is a consequence of the requirement of the force balance that yields non-trivial correlations between the components of the Hessian. As



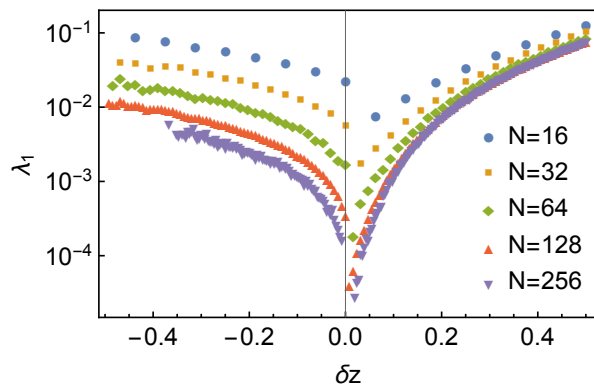


FIG. 12.  $\delta z$  dependence of the first eigenvalue  $\lambda_1$  for  $\sigma = -0.5$ . The markers denote the numerical results of the average value of  $\lambda_1$ .

this is a quite general mechanism for the models driven by the gradient descent dynamics, our result raises a serious question about the usefulness of the conventional stability analysis for complex systems based on random matrix with uncorrelated elements [27, 28]. Further studies are necessary along this line.

We find that the cost function exhibits exponential decay in the SAT phase. In particular, the relaxation time remains finite even in the non-convex phase. We would like to stress that this is qualitatively different from the UNSAT phase. To see this point more concretely, in Fig. 12, we show the  $\delta z = 1 - z$  dependence of the first eigenvalue  $\lambda_1$ , which is inversely proportional to the relaxation time. One can see that in the SAT phase  $\delta z > 0$ ,  $\lambda_1$  converges to a finite value in the thermodynamic limit  $N \rightarrow \infty$  except very near the transition point  $\delta z \ll 1$ , in particular, the data for  $N = 128$  and  $N = 256$  are

almost indistinguishable in the linear scale. On the contrary, in the UNSAT phase  $\delta z < 0$ ,  $\lambda_1$  exhibits significant finite size effects even far from the transition point. This strong  $N$  dependence in the UNSAT phase is fully consistent with the previous theoretical result based on the replica method, which predicts that the eigenvalue distribution in the non-convex UNSAT phase is gapless in the thermodynamic limit [20]. This result gives some theoretical background on the efficiency of the learning of neural networks in the overparameterized region over that in the underparameterized region.

The perceptron model investigated here belongs to the same universality class of spherical particles in the large dimensional limit [7]. From a practical point of view, it is important to introduce the effect of asphericity, as real granular particles are in general non-spherical. Moreover, there is a recent study that reports some class of multilayer perceptron exhibits similar empirical observations near the SAT-UNSAT phase transition to those of the jamming of ellipsoids [29]. In previous works, we have shown that the eigenvalue distribution of ellipsoids is significantly different from that of spherical particles [30–32]. It would be interesting to see how this difference affects the dynamics.

## ACKNOWLEDGMENTS

We thank F. Zamponi, A. Ikeda, E. DeGiuli, A. Altieri and P. Urbani for kind discussions. We also thank G. Biroli for useful comments. This project has received funding from the European Research Council (ERC) under the European Union’s Horizon 2020 research and innovation programme (grant agreement n. 723955-GlassUniversality).

- 
- [1] S. Kirkpatrick, C. D. Gelatt, and M. P. Vecchi, *science* **220**, 671 (1983).
  - [2] H. Nishimori, *Statistical physics of spin glasses and information processing: an introduction*, 111 (Clarendon Press, 2001).
  - [3] M. Mezard, M. Mezard, and A. Montanari, *Information, physics, and computation* (Oxford University Press, 2009).
  - [4] S. Franz, G. Parisi, M. Sevelev, P. Urbani, F. Zamponi, and M. Sevelev, *SciPost Physics* **2**, 019 (2017).
  - [5] F. Rosenblatt, *Psychological review* **65**, 386 (1958).
  - [6] E. Gardner and B. Derrida, *Journal of Physics A: Mathematical and general* **21**, 271 (1988).
  - [7] S. Franz and G. Parisi, *Journal of Physics A: Mathematical and Theoretical* **49**, 145001 (2016).
  - [8] E. Agoritsas, G. Biroli, P. Urbani, and F. Zamponi, *Journal of Physics A: Mathematical and Theoretical* **51**, 085002 (2018).
  - [9] Y. LeCun, Y. Bengio, and G. Hinton, *nature* **521**, 436 (2015).
  - [10] M. A. Nielsen, *Neural networks and deep learning*, Vol. 25 (Determination press San Francisco, CA, USA, 2015).
  - [11] D. Soudry and Y. Carmon, *arXiv preprint arXiv:1605.08361* (2016).
  - [12] Z. C. Lipton, *arXiv preprint arXiv:1602.07320* (2016).
  - [13] Y. Cooper, *arXiv preprint arXiv:1804.10200* (2018).
  - [14] M. S. Advani and A. M. Saxe, “High-dimensional dynamics of generalization error in neural networks,” (2017), *arXiv:1710.03667*.
  - [15] F. Draxler, K. Veschgini, M. Salmhofer, and F. A. Hamprecht, *arXiv preprint arXiv:1803.00885* (2018).
  - [16] M. Geiger, A. Jacot, S. Spigler, F. Gabriel, L. Sagun, S. d’Ascoli, G. Biroli, C. Hongler, and M. Wyart, *arXiv e-prints*, *arXiv:1901.01608* (2019), *arXiv:1901.01608 [cond-mat.dis-nn]*.
  - [17] P. Olsson and S. Teitel, *Physical review letters* **99**, 178001 (2007).
  - [18] A. Ikeda, T. Kawasaki, L. Berthier, K. Saitoh, and T. Hatano, *arXiv preprint arXiv:1904.07359* (2019).
  - [19] E. Lerner, G. Düring, and M. Wyart, *EPL (Europhysics Letters)* **99**, 58003 (2012).
  - [20] S. Franz, G. Parisi, P. Urbani, and F. Zamponi, *Pro-*

- ceedings of the National Academy of Sciences **112**, 14539 (2015).
- [21] This would be not true for larger  $|\sigma|$  for  $\sigma < 0$  where the difference between the RS result and the the RSB result is significant so one cannot rely on the RS result.
  - [22] A. Altieri, S. Franz, and G. Parisi, *Journal of Statistical Mechanics: Theory and Experiment* **2016**, 093301 (2016).
  - [23] L. Yan, E. DeGiuli, and M. Wyart, *EPL (Europhysics Letters)* **114**, 26003 (2016).
  - [24] M. Müller and M. Wyart, (2015).
  - [25] P. Charbonneau, J. Kurchan, G. Parisi, P. Urbani, and F. Zamponi, *Nature communications* **5**, 3725 (2014).
  - [26] G. Livan, M. Novaes, and P. Vivo, *Introduction to random matrices: theory and practice* (Springer, 2018).
  - [27] R. M. May, *Nature* **238**, 413 (1972).
  - [28] Y. LeCun, I. Kanter, and S. A. Solla, in *Advances in neural information processing systems* (1991) pp. 918–924.
  - [29] M. Geiger, S. Spigler, S. D’Ascoli, L. Sagan, M. Baity-Jesi, G. Biroli, and M. Wyart, *Physical Review E* **100**, 012115 (2019), arXiv:1809.09349.
  - [30] C. Brito, H. Ikeda, P. Urbani, M. Wyart, and F. Zamponi, *Proceedings of the National Academy of Sciences* **115**, 11736 (2018).
  - [31] H. Ikeda, P. Urbani, and F. Zamponi, *Journal of Physics A: Mathematical and Theoretical* **52**, 344001 (2019).
  - [32] H. Ikeda, C. Brito, and M. Wyart, arXiv preprint arXiv:1908.02091 (2019).